Thermochemical energy storage in $CaCl_2$-NH_3 pair evaluated by rapid multiple adsorption-desorption cycles controlled with wasted iron induction heating

Siudyga, Tomasz; Wojtacha-Rychter, Karolina; Anagnostopoulos, Argyrios; Navarro, Helena; Ding, Yulong; Smolinski, Adam; Magdziarczyk, Malgorzata; Mierczynski, Pawel; Polanski, Jaroslaw

DOI:
10.1016/j.measurement.2023.113420

Document Version
Publisher's PDF, also known as Version of record

Citation for published version (Harvard):
Siudyga, T, Wojtacha-Rychter, K, Anagnostopoulos, A, Navarro, H, Ding, Y, Smolinski, A, Magdziarczyk, M, Mierczynski, P & Polanski, J 2023, 'Thermochemical energy storage in $CaCl_2$-NH_3 pair evaluated by rapid multiple adsorption-desorption cycles controlled with wasted iron induction heating', *Measurement*, vol. 220, 113420. https://doi.org/10.1016/j.measurement.2023.113420

Measurement 220 (2023) 113420

Contents lists available at ScienceDirect

Measurement

journal homepage: www.elsevier.com/locate/measurement

Thermochemical energy storage in $CaCl_2$-NH_3 pair evaluated by rapid multiple adsorption-desorption cycles controlled with wasted iron induction heating

Tomasz Siudyga [a], Karolina Wojtacha-Rychter [b], Argyrios Anagnostopoulos [a,c], Helena Navarro [c], Yulong Ding [c], Adam Smolinski [b,d,*], Malgorzata Magdziarczyk [e], Pawel Mierczynski [f], Jaroslaw Polanski [a]

[a] Faculty of Science and Technology, Institute of Chemistry, University of Silesia, Szkolna 9, 40-006 Katowice, Poland
[b] Central Mining Institute, Plac Gwarkow 1, 40-166 Katowice, Poland
[c] University of Birmingham, School of Chemical Engineering, Birmingham, United Kingdom
[d] Spolka Restrukturyzacji Kopaln S.A., Strzelcow Bytomskich 207, Bytom, Poland
[e] Opole University of Technology, Faculty of Economics and Management, Luboszycka 7, 45-036, Opole, Poland
[f] Lodz University of Technology, ul. Żeromskiego 116, 90-924 Łódź, Poland

A B S T R A C T

Energy storing systems can provide leverage to the current supply demand intermittency issue thus increasing energy efficiency. Among many available technologies, thermochemical energy storage is highly promising. In this work, we investigate, experimentally, for the first time, inductive heating as an approach to direct coupling of power systems with thermal energy technologies. This system also allows for versatile measurements in rapid multiple adsorption–desorption cycle control. Adsorption and desorption cycling of the $CaCl_2$-NH_3 adducts is realized in a custom-made setup. Iron wires and waste red mud are investigated as potential inductive materials. Material performance is evaluated after 1, 2 and 1000 cycles using differential scanning calorimetry, thermogravimetry, scanning electron microscopy and specific surface area. Waste red mud shows good inductive potential. No material degradation is observed after 1000 cycles in all cases. Samples heated using waste red mud have a higher maximum absorption capacity (0.304 versus 0.154 g_{NH3}/g_{CaCl2}) and desorption enthalpy (716 versus 460 KJ/ kg_{CaCl2}) compared to the ones heated using iron wires. This is found to be related to the average specific surface area of samples containing red mud, which is almost double that of iron ones. We hope the concept presented here can stimulate research in the direction of inductive heating while simultaneously generating new utilization pathways for waste red mud.

1. Introduction

Thermal energy with different parameters constitute 40–60% of the final energy consumption in most economies today [1]. Currently, much attention is focused on its effective use. On the other hand modern, dynamic lifestyles coupled with an increase in renewable energy penetration in the power production mix have resulted in an increased supply–demand intermittency issue [2]. This issue can be resolved through low-cost energy storage technologies capable of accommodating for the power, energy and seasonality of the demand-side [3]. Hence, thermal energy storage (TES) is such a technology, that can be used to increase peak shaving performance of energy networks [3].

There are three types of TES technologies, sensible, latent and thermochemical. Thermochemical energy storage (TCS) has between 8 and 20 times higher storage density than sensible and latent based TES technologies[4]. This feature has rendered it a promising prospect and has resulted in considerable research focus in the past decade. However, despite efforts, its technology readiness level is still predominantly at the material stage [5]. TCS faces several issues related to material lifespan due to poor stability, as well as high material cost [4]. These coupled with presently inefficient reactor designs hinder the market uptake of TCS.

This work is focused on domestic applications. In these temperature ranges (between −50 and 150 °C) sorption reaction pairs are most promising [6]. In such reactions, the heat stored in chemical and physical bonds formed between a sorbent and a sorbate could be restored in the retrieval step giving back the energy. Common sorbents are salt hydrates, activated carbons, aluminophosphates, zeolites, metal–organic frameworks (MOFs) or metal halides, while sorbates are commonly water vapor, ammonia, ethanol or methano [7]. Ethanol and

* Corresponding author at: Central Mining Institute, Plac Gwarkow 1, 40-166 Katowice, Poland.
E-mail address: smolin@gig.katowice.pl (A. Smolinski).

https://doi.org/10.1016/j.measurement.2023.113420
Received 8 June 2023; Received in revised form 27 July 2023; Accepted 5 August 2023
Available online 12 August 2023

methanol systems are highly toxic and flammable [8]. Ammonia based systems offer higher energy storage densities than the water-based systems and more flexibility in the system operating pressures.

Amongst the various reactants types, ammoniates present an advantage on heat and mass transfer against hydrates because of the higher pressure levels at which these working pairs operate [9]. A variety of metal halides has been tested as potential sorbents for NH_3 based TES. These include NaBr, $CaCl_2$, $SrCl_2$, $MnCl_2$, $FeCl_2$. Ammonia sorption occurs in different temperature ranges for individual halides, so it allows using thermal energy with very different parameters (temperature) - also by using their mixtures. Among these $CaCl_2$ is especially interestng. It is a waste-type byproduct resulted from hydrometallurgy processes [10–13] or sodium carbonate production [14]. As such, it's a broadly available, low cost and low toxicity option. On the other hand, ammonia sorption on this chemical compound occurs in a wide range of temperatures, which makes it a material with many applications in thermal energy storage systems.

There are several studies in the literature on the $CaCl_2$-NH_3 working pair. Van der Pal and Critoph performed experimental tests and developed a numerical model for a reactor consisting of 1 kg of $CaCl_2$ and 1 kg of expanded natural graphite (ENG) [10]. Oliveira et al. and Wang et al. developed a $CaCl_2$-based system for refrigeration purposes (ice making) [11,12]. Sakamoto and Yamamoto examined the influence of Ti (Titanium) on the heat transfer rate of the solid ammoniated salt ($CaCl_2$-mNH_3) [13]. $CaCl_2$-NH_3 was described previously as the TES system and for the potential NH_3 storage in the form of solid pre-fuel [14]. Zisopoulos et al. investigated computationally a heat pump, for domestic heating and cooling, based on $CaCl_2$-NH_3 and found a minimum COP of 3.63 [15].

Apart from its implementation in a thermomechanical energy storage (TEMS) system TCM can be used in direct power to heat systems. Direct connection of power to heat is quite promising, compared to other options, given the cost and challenges of on demand generation of heat through electricity coupled with the low cost of TES [16]. Converting electrical energy directly into heat without any mechanical transformations can also be achieved through direct induction systems.

The originality of the current work lies on the study of new TCS system based on the inductively controlled under isochoric and isobaric condition. Induction heating is the process of heating electrically conductive materials by means of electromagnetic induction. An important feature of this heating process is efficiency, non-contact, precise, repeatable process, and by that the heat is generated inside the object itself, instead of an external heat source via heat conduction. Recently, the efficiency of direct inductive heating was demonstrated in organic synthesis (e.g. Suzuki–Miyaura and Heck coupling reactions) [17]. Just recently, we showed how this method could be used in the sustainable methane production via carbon dioxide hydrogenation in Ru-Ni nanocatalysis [18].

In this work, we investigate, experimentally, for the first time, inductive heating as an approach to the direct coupling of power systems with thermal energy technologies. This system also allows for versatile measurements in rapid multiple adsorption–desorption cycle control. Here we explored a red mud as a potential ferromagnetic material to generate heat through induction in charging step. And to our best knowledge this is also the first reported attempt of alumina refinery waste (red mud) management in the low-temperature thermochemical heat storage. Red mud (RM) is an industrial waste of the aluminum industry with a 150 Mt/year worldwide production [19]. Its disposal is facilitated typically in dykes/dams or alternatively directly in the sea posing a considerable environmental impact due to its high alkalinity 11.3 ± 1 and traces of heavy metals [20]. RM has a large content of iron oxide, 20–50 wt% depending on its origin and processing method [21,22]. Magnetic separations revealed, γ-Fe_2O_3 in major amounts along with other matrix incorporated phases, such as Fe_2TiO_4, SiO_2, and Al_2O_3, mostly in amorphous form. This magnetically active agglomerate particle presented anodic functions and was been found to perform well in Li-ion batteries [23]. Due to the difficulties in Red Mud utilization, its use in thermal energy storage systems would open up new possibilities in this area by using its ferromagnetic properties.

In this study, halide salt powder ($CaCl_2$) as thermochemical storage material was mixed with the waste red mud as the inductive element. $CaCl_2$/red mud-NH_3 adducts are placed in the cooper coil and rapidly heated to high temperature by induced currents from the highly concentrated magnetic field. Under the influence of a heat supply, a working pair is decomposed into separate components, which can be stored separately. TCS working pair was inductively cycled as many as 1000 times. The structure and thermal performance were inspected at various cycling times using followed analytical techniques: temperature-programmed desorption (TPD), TG, DSC and scanning electron microscopy (SEM) with EDS, analyses.

Direct inductive heating of the in-powder-$CaCl_2$-NH_3 pair lets us keep mass and heat transfer at efficient levels without any need for further processing at the material stage such as adsorbent pelletizing or structuration by introducing an additional porous solid matrix.

Table 1
Prices of low purity metal salts reported in previous TCS studies (source [a]).

Entry	Salt	Price USD/Tone
1	$CaCl_2$	100
2	NaBr	700
3	$SrCl_3$ $6H_2O$	650
4	$MnCl_2$ $4H_2O$	1600
5	$FeCl_2$ $4H_2O$	1350

[a] https://https://www.made-in-china.com/products-search/hot-china- products/Calcium_chloride_Price.html.

Table 2
The content of principal elements identifed in the RM sample used in this work.

Element (-)	O	Fe	Ca	Al	Ti	Si	Na	V
Atomic (%)	53.15	10.77	4.51	5.55	1.75	2.32	1.89	0.05
Weight (%)	14.37	10.16	3.06	2.53	1.42	1.10	0.74	0.04

2. Materials and methods

2.1. Materials

Material cost is one of the bottlenecks of TCS. Table 1 lists the prices of low purity salts commonly investigated as candidates in TCS systems. Among these, $CaCl_2$, is the lowest price alternative. To this end it is selected for this work.

In order to prepare samples for the tests the commercial anhydrous $CaCl_2$ (analytically pure, Chempur, CAS 10043–52-4) is first dried at 110 ℃ for 1 h or calcinated at 500 ℃ for 1 h.

Iron wires (100 mg) and/or an RM (100 mg) were employed as ferromagnetic component. RM is found to be able to potentially replace iron as the inductive active material. The RM sample used in this study was sourced from the company "Aluminium of Greece" and particularly from its production facilities located in Boeotia, Greece. It contains as much as 40% iron oxide, a significant quantity of silica (15.78%), some amount of aluminum and calcium oxides (11.79% and 10.97% respectively) as seen in Table 2[24,25]. X-ray powder diffraction (XRD) and scanning electron microscope (SEM) analysis is conducted to identify the most crystalline phases of iron (III) oxide, such as hematite (α-Fe_2O_3), maghemite (γ-Fe_2O_3) and magnetite (Fe_3O_4).

As expected (Fig. 1), the predominant minerals of the RM tested is hematite (α-Fe_2O_3), but the relative amounts of calcite ($CaCO_3$), cancrinite ($Na_8(Al_6Si_6O_{24})((CaCO_3)_2)$), and corundum (as a crystalline form of Al_2O_3) are also relevant. It means that iron in the RM is in the form of hematite and andradite, calcium exists mainly in the form of calcite and cancrinite, aluminum in the form of corundum, and sodium comes

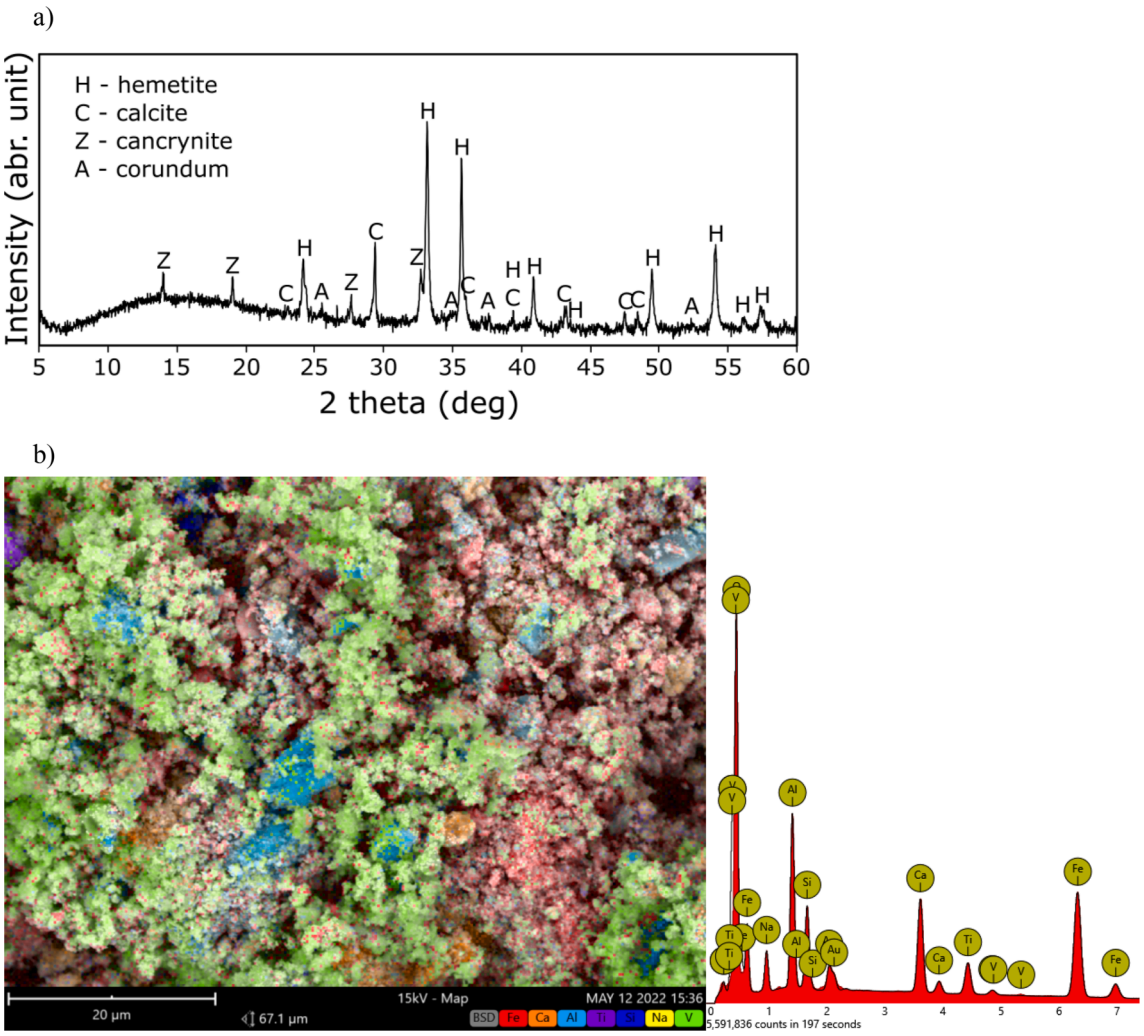

Fig. 1. Mineralogical composition of a red mud sample used (a) and SEM-EDS analysis of red mud component (b).

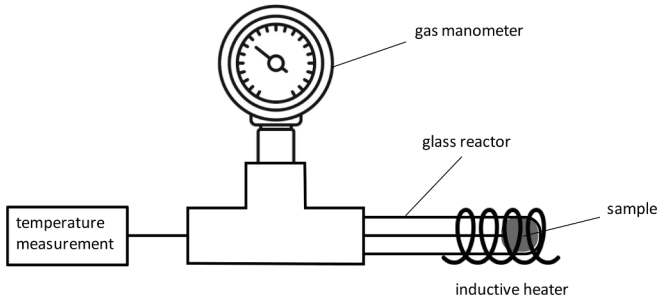

Fig. 2. The TES installation with inductive heating for $CaCl_2/NH_3$ processing.

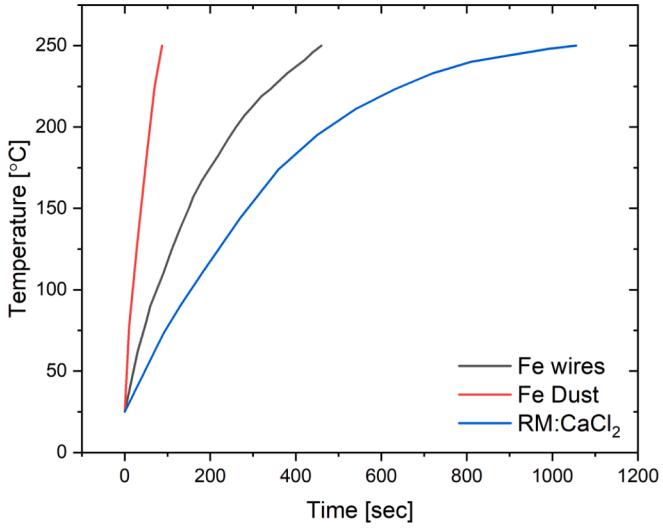

Fig. 3. Inductive heating profiles for the ferromagnetic components (Fe wires and dust) and the red mud.

mainly from cancrinite.

SEM analysis shows that RM is composed of a mixture of loose coarse and fine particles with varying degrees of agglomeration (Fig. 1). The average particle size of the RM is below 20 µm. In addition, the elemental analysis relating to Fig. 3 is reported in Table 2, confirms that the prominent constituent of red mud is found to be iron with its oxides, which is in accord with the elemental composition analysis of red mud by using XRD. High iron content indicates that the analyzed RM originated form a Bayer processing, which constitutes the majority of aluminum production [30,31]. It was found that the iron element on the RM surface is strongly associated with iron vanadium oxide (seen as green color on the EDS map) and hematite (red color on map), which have regular and sharp-edged shapes respectively. EDS signatures of Ca and Al accompanied by Si, Ti, Na, and V indicate the presence of specific minerals sodium aluminosilicate, aragonite, calcite, boehmite and

perovskite.

2.2. Isochoric and isobaric TES equipment with inductive heating

A custom-made experimental setup is used for NH_3 adsorption/desorption tests (Fig. 2). A coil is wrapped around the glass reactor and connected to a custom-made in-lab inductive heating system consisting of a controller with enabled an automatic on/off function at different time intervals. The maximum induction heating power is 100 W. A total of 100 mg of sample are introduced in the glass reactor. For inductive heating ferromagnetic components are introduced directly into $CaCl_2$. Formally, $CaCl_2$:Fe mass ratio for samples FV, F1, FK and F1KS was 1:1 ($CaCl_2$:Fe molar ratio 1:1.985). For samples RV, R1, RK and R1KS, $CaCl_2$:RM mass ratio was also 1:1 ($CaCl_2$:Fe molar ratio 1:0.202 due to lower Fe content in the RM).

The experiments were conducted under isochoric conditions (constant volume), established through a manometer that monitors pressure changes. It was also considered experiments at constant pressure, enforced through a gas syringe, with a capacity of 100 mL. Due to the ease of ensuring a constant volume the isochoric conditions were selected. Ammonia adsorption was completed when the pressure value of the manometer stabilized. Average adsorption equilibration time in this system was 1 h, which was in agreement with previous literature reports.

TES systems have long lifetimes and are expected to operated without considerable maintance for up to 25 years. One of the bottlenecks of TCS systems is long term stability and performance. For a TCS system to reach commercialization it should be extensively cycled. To this end the lab setup is used to evaluate the long term stability of the material through thermal cycling. To avoid ammonia leaks during extensive cycling, the system is refilled with ammonia every ~100 cycles.

Inductive heating allows for rapid and efficient heating/cooling. A complete NH_3 adsorption/desorption is carried out after 90, 400 and 900 sec in the case of the iron wires, iron dust and RM respectively. The inductive behaviour of ferromagnetic components is a complex issue which depends on the composition, shape and granularity of the individual material. which explained the difference between iron wires and dust [26]. Iron wires are selected based on their higher performance. The longer heating rate in the case of RM reflects its magnetic properties. The magnetic susceptibility of RM is in the range of hematite, which is the primary iron phase identified in RM [27]. The magnetic permeability of magnetite (iron wires) is between 2.5 and 16 times that of hematite [28]. Nevertheless, these heating profiles indicate that RM could potentially replace iron dust and even iron wires with proper processing and insulation (Fig. 3).

Following the heating step using the induction coil is a cooling step (600 sec) to ambient conditions using an electric fan. After 1000 cycles, the material is extracted from the glass reactor and subjected to temperature-programmed desorption (TPD), TG, DSC and scanning electron microscopy (SEM) with EDS, analyses.

Additionally, a second set of tests are conducted with the material placed in the reactor in tightly sealed tube. $CaCl_2$ is first impregnated with NH_3 for 1 before sealing. The ratio $CaCl_2$ to ferromagnetic ratio is identical to that of the unsealed systems.

2.3. Temperature-programmed desorption TPD

The TPD measurements are carried out in a quartz reactor using NH_3 as a probe agent (NH_3-TPD). The NH_3 is adsorbed on the samples at 25 °C for 30 min after purification of catalyst surface in flowing He at 500 °C for 60 min. The temperature programmed desorption of NH_3 was carried out in the temperature range 25–500 °C using a linear growth of temperature (27 °C min^{-1}) and a thermal-conductivity detector.

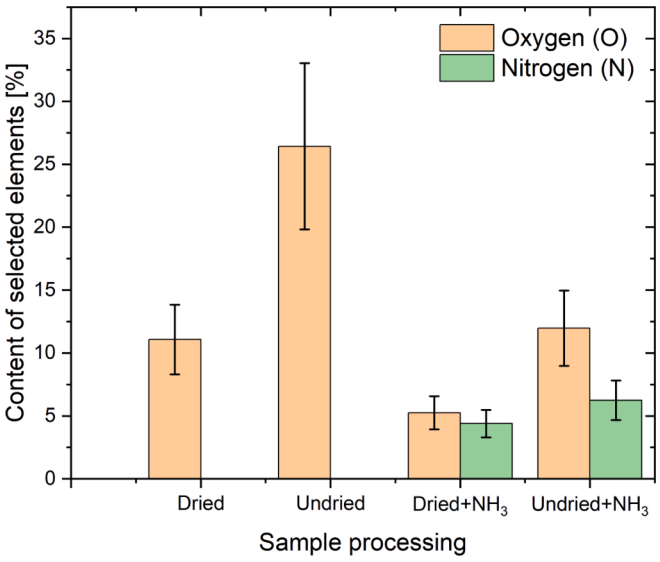

Fig. 4. EDS analysis of selected elements in calcium dried and undried calcium chloride samples before and after processing with NH_3.

2.4. DSC and TG analyses

Thermogravimetric analysis was performed on TGA/DSC 3+ (Mettler-Toledo) instrument. The TGA-DSC measurements in the range of 30 to 350 °C or 1100 °C are performed with the linear heating rate of 20 °C·min^{-1} with a flow of synthetic air and nitrogen (80 mL·min^{-1}).

2.5. Scanning electron microscopy (SEM)

The Phenom XL (Thermo Fisher Scientific, USA) Scanning Electro Microscope (SEM), equipped with the secondary electron (SE) detector fixed to the magnifications of 1000X and 4000X, is used to map the surface morphology and analyse the chemical composition of the samples.

2.6. X-ray powder diffraction (XRD)

Powder aggregates are analyzed in terms of the phase composition by means of Philips X-ray powder diffraction X'Pert system (CuKα radiation). Measurements are carried out in the 2θ angle range of 5–90° for 2 h, with a step size of 0.001. Phases are identified using the X'Pert HighScore Plus software, and compared with data from the International Centre for Diffraction.

3. Results and discussion

$CaCl_2$ is both hygroscopic and deliquescent meaning it can absorb moisture from the air, to the point of converting to liquid brine[29]. In fact, an oxygen content of 25% is identified on the surface of the commercial anhydrous $CaCl_2$, through EDS analysis (Fig. 4). After drying the oxygen content is still 11.1%. Water adsorption results in the absence of grain boundaries, and consequentially in a continuous structure with a reduced porosity. The water-induced agglomeration of $CaCl_2$ is well known and described in the literature and can inhibit ammonia transport [30].

Both dried and undried samples are treated with ammonia at 110°C for 1 h followed by another 1 h at ambient temperature. However, even after exposure to ammonia (virgin $CaCl_2$), reflected by the N content, traces of water are still present on the $CaCl_2$ surface. What is surprising is the nitrogen, and hence ammonia, content is higher in the undried sample. This could suggest that above a certain threshold the water content does not affect ammonia absorption.

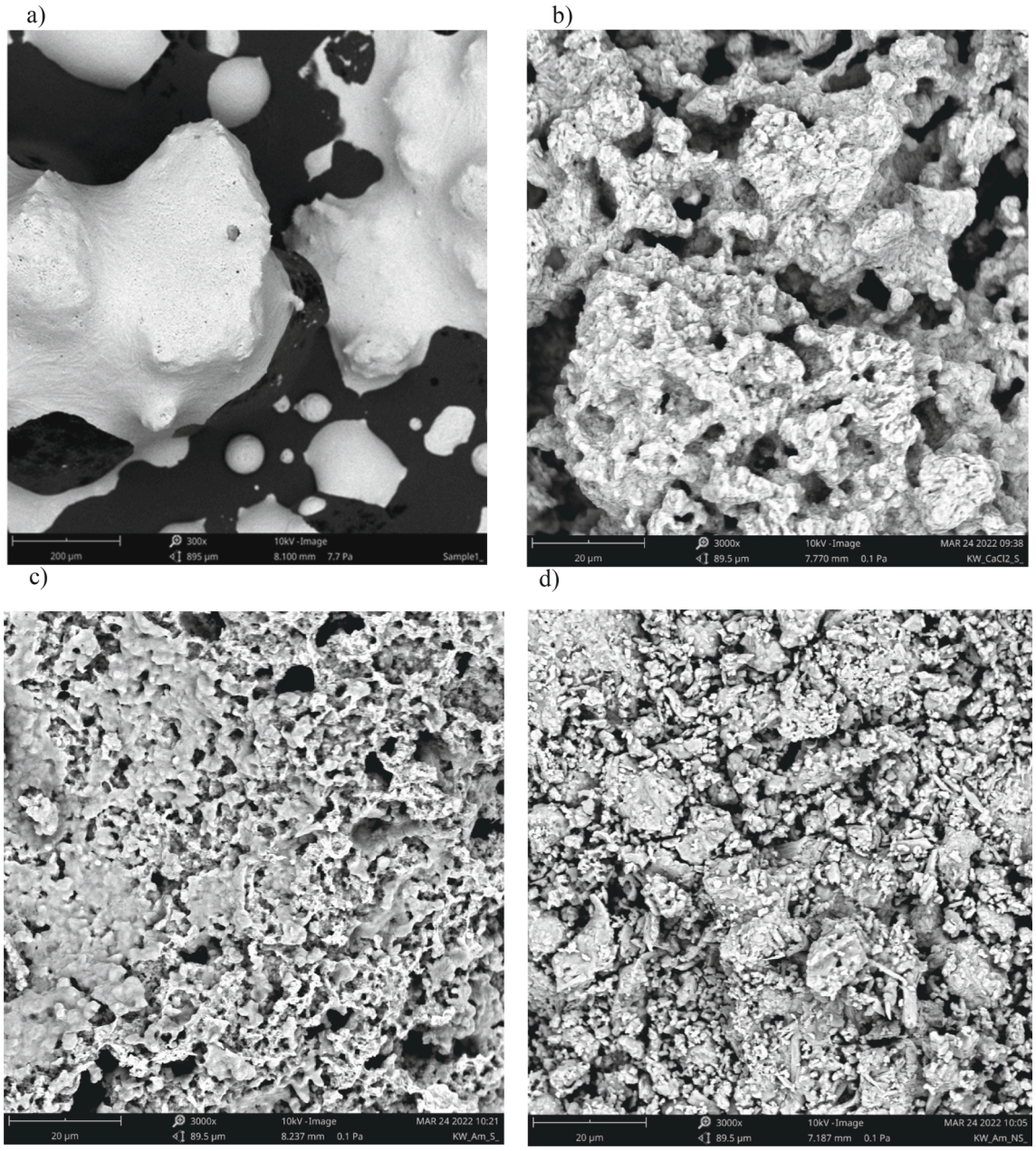

Fig. 5. SEM images of commercial undried $CaCl_2$ (a), dried $CaCl_2$ (b), $CaCl_2$ dried and treated with NH_3 (c) and undried $CaCl_2$ treated with NH_3 (d).

Water content is also identified via SEM (Fig. 5). A porous surface area is visible in the dried $CaCl_2$. On the contrary, undried $CaCl_2$ has a visually denser, skull like morphology. Chemical composition analysis of individual spots confirms that the more skull-like sectors are linked to water agglomerates, while the middle size structures, or small cubic formations could be assigned to ammonium rich $CaCl_2$ adducts. This effect may block ammonia transport through the pores. Exposure to ammonia is evident in the form of crystallites of varying sizes that cover the porous surface.

Interestingly, extended cycling did not diminish the absorption capacity. The TPD-profiled after 1 and 1000 (1 K) cycles are almost identical (Fig. 6). The TPD profiles indicate that NH_3 adsorption takes place in two different phases forming a low and high-temperature peak. The maxima for these peaks can slightly differ depending on the individual samples. What is notable is that the peak desorption temperatures decrease with increasing number of cycles. This is probably because cycling increases porosity (see below) and therefore enhance mass transfer.

With respect to sorption capacity the base values of virgin iron containing samples is in proximity with literature reports (Fig. 7). The issue is that all these values are quite distant from the theoretical adsorption capacity at room temperature observed, which for $CaCl_2$ is 1.228 g_{NH3}/g_{CaCl2} [31]. There are currently ongoing efforts to improve capacity particularly in the field of ammonia synthesis [32]. Results show that sorption capacity is also increased with cycling. The amount of NH_3 adsorbed is about 47% higher after 1000 cycles in the case of iron and 146% in the case of RM (Fig. 8.a). This effect is most likely related to the availability of the ammonia excess in pretreatment (fatigue tests) that removes residual water adsorbed at the $CaCl_2$ surface coupled with increased porosity, which increases surface availability. Competition between water and ammonia results in replacing water agglomerates with ammonia formations. As a result, ammonia blocks $CaCl_2$ surface from water sorption and enables easier ammonia adsorption. Interestingly, this effect cannot be observed even after intense drying because

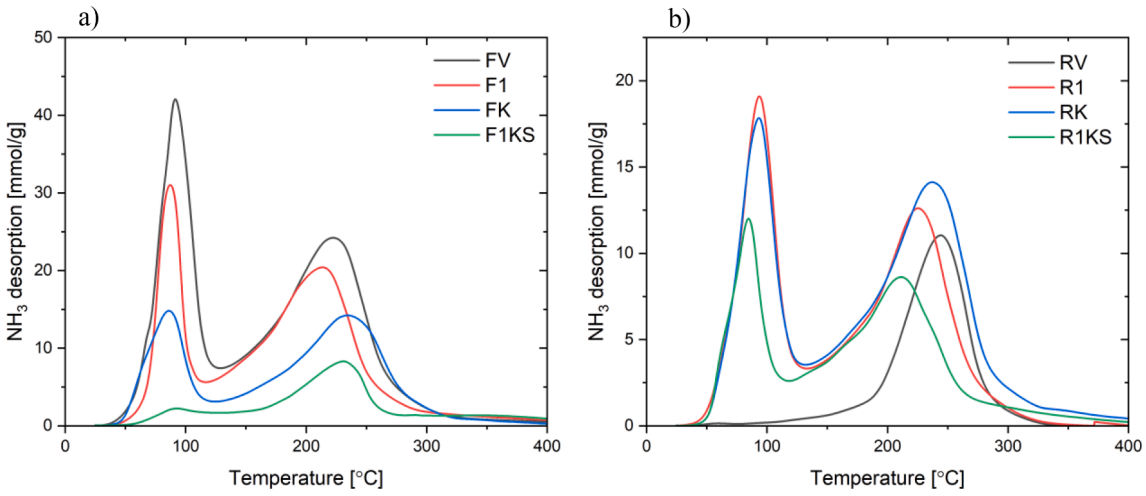

Fig. 6. TPD measurements of inductively heated with iron (a) and red mud (b).

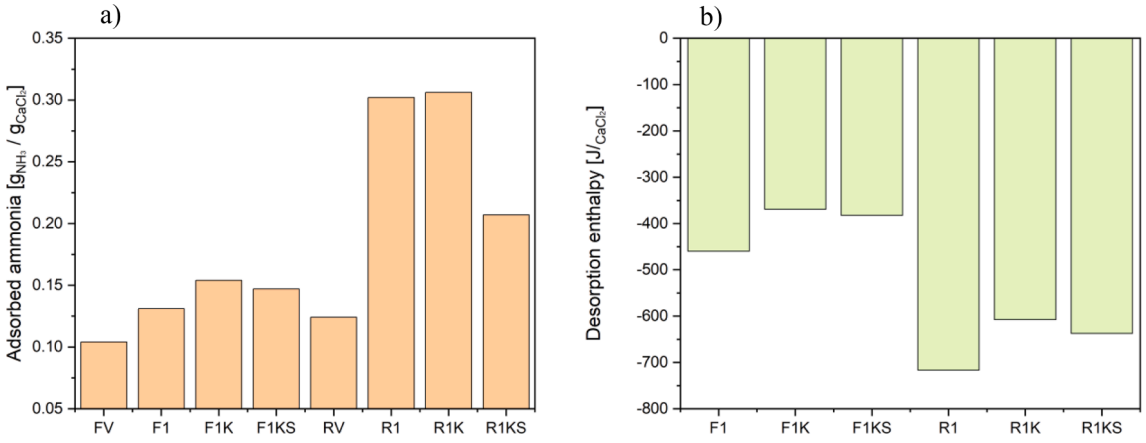

Fig. 7. Total amount of ammonia adsorbed (a) and desorption enthalpy (b) for all investigated samples. F: denotes iron, 1: 1 cycle, 1 K: 1000 cycles, R: red mud and S: sealed.

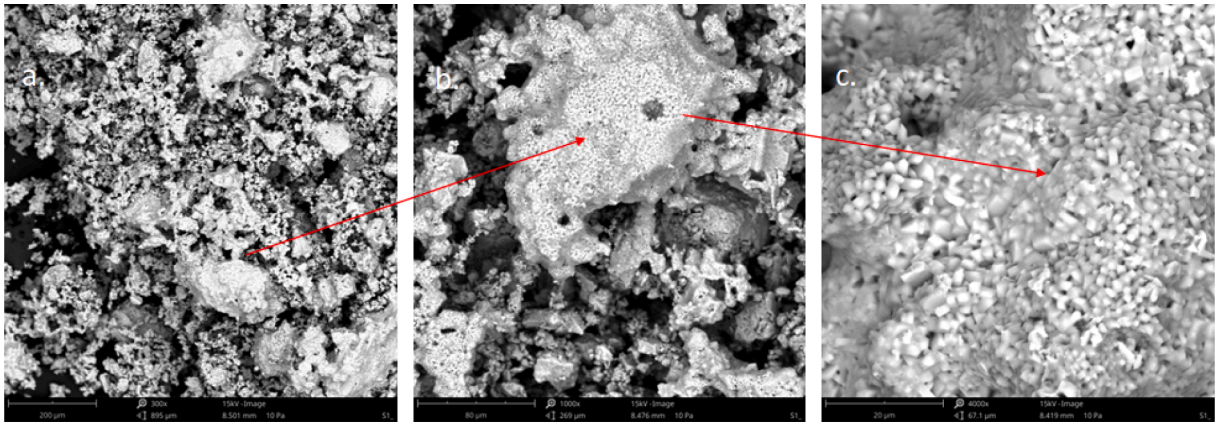

Fig. 8. SEM snapshots of virgin $CaCl_2$ (dried $CaCl_2$ exposed to ammonia).

$CaCl_2$ surface without NH_3 surface protection immediately attracts water from the environment. To compare the energy levels of the products obtained by the reaction of $CaCl_2$ with two different sorbents (ammonia and water), the Gibbs free energies of the two processes at 30C were calculated using equation (1):

$$\Delta_r G = \Delta_r H - T\Delta_r S, \quad (1)$$

where the enthalpy of reaction $\Delta_r H$ and the change of entropy of the reaction $\Delta_r S$ have been found in the literature [33,34,35,36]. Obtaining for reactions

$$CaCl_2 \bullet 2H_2O + 2H_2O(g) = CaCl_2 \bullet 4H_2O$$

$$CaCl_2 \bullet 2NH_3 + 2NH_3(g) = CaCl_2 \bullet 4NH_3$$

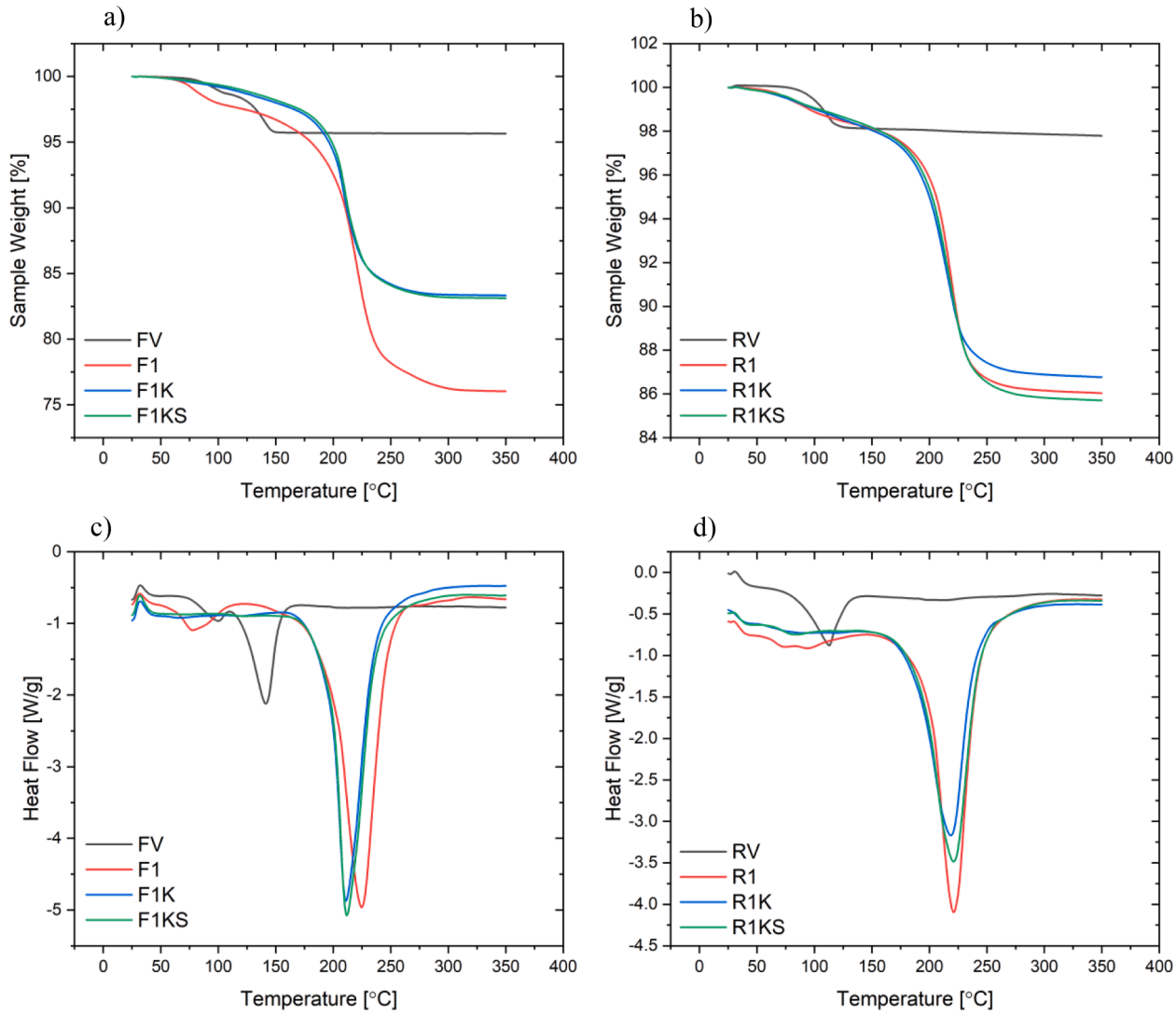

Fig. 9. TGA (a,b) and DSC (c,d) curves for iron (a,c) and RM (b,d) samples.

That for ammonia reaction $\Delta_r G$ is −3.9 kJ and for water sorption is −36.01 kJ. This indeed verifies that in a surface where ammonia has not been adsorbed the salt attracts water faster. This is further evidenced by the NH_3-TPD profiles of the virgin $CaCl_2$ samples (Fig. 6, black lines) where the low temperature desorption peak is non present in the case of RM and barely visible in iron. This indicates the presence of a barrier of skull-like structures both to absorption and desorption phases. In fact in SEM images of virgin $CaCl_2$ cubic shapes can be visualized, which, tend to be a part of the extensive network of the large, not well-defined skull-like surface structure (Fig. 8). Oxygen traces are identified through chemical composition analysis in marked areas (Fig. 8, middle). Although $CaCl_2$ dehydration is anticipated at high temperatures, that is only partial, which is a well-known effect in $CaCl_2$ chemistry.

In the case of the sealed sample, adsorption capacity is increased but by much lower rates; 36% and 82% for iron and red mud respectively. This is probably due to the fact excess ammonia was introduced every 150 cycles in the unsealed samples to avoid potential losses. However, in the tightly sealed experiment, the sample is exposed to a stable level ammonia. The highest adsorption capacity of 0.306 g_{NH3}/g_{CaCl2} is achieved in the R1K sample. This value is 1/3 of the highest theoretical level. Nevertheless, is still quite promising even accounting for the mass of the RM (~50%). In fact, studies using covalent organic frameworks to enhance the absorption capacity of $CaCl_2$ report values below that [37]. It is certainly not the highest value currently reported [38], but given the fact that this is achieved by simple mixing and no complex material engineering is required makes RM a potential by-product for ammonia capture related applications.

Further to the NH_3-TPD TG and DSC analyses of the virgin and NH_3 cycled $CaCl_2$ samples are also conducted (Fig. 9). Unlike NH_3-TPD, where the NH_3-$CaCl_2$ adducts in situ directly under the NH_3-TPD experiment, in the TG and DSC, the NH_3-$CaCl_2$ samples are removed from the TES installation analyzed without any further processing. In fact contrary to adsorption capacity desorption enthalpy, measured by DSC, is slightly lower after extensive cycling. This effect is of analogous magnitude in both RM and iron (Fig. 8 left). This is probably due to water absorption by $CaCl_2$ during transfer from the custom made cycling setup to the measurement apparatus.

Contrary to the TDP in the DSC only a single high temperature signal at 220°C is observed. The low-temperature effect observed in NH_3-TPD is absent. Most likely the NH_3-$CaCl_2$ adducts removed from the TES system slightly decomposed before TG and DSC testing. Similarly to NH_3-TPD a slight shift in the desorption peak maxima towards lower temperatures is observed when comparing the cycled samples with base.

Interestingly, the inductive heating of the NH_3 treated samples with red mud appeared more efficient than heating with iron wires, even though the ferromagnetic component of red mud is relatively low. A fine structured red mud allows for a better, more uniform, and efficient heat transfer within the TES system.

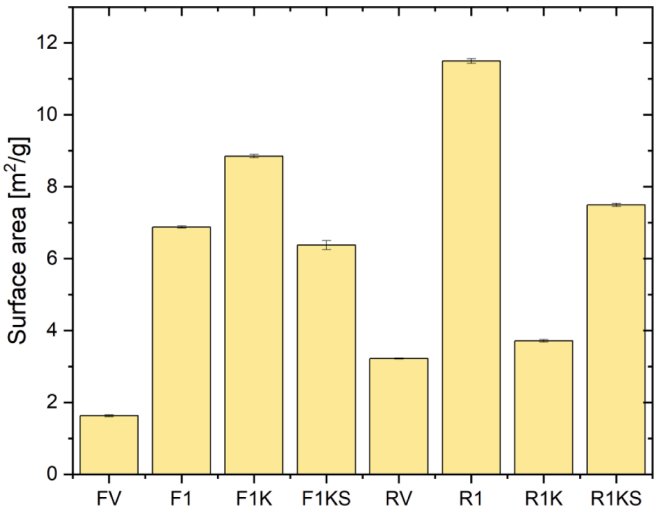

Fig. 10. $CaCl_2$ sample used in the TES cycling.

This is reflected by the on average, higher surface area in the RM samples (Fig. 10), which suggests better mass transfer and thus enhanced ammonia transport in $CaCl_2$.

A more pronounced pore network of NH_3 adducts is evident in red mud samples in agreement with BET measurements (Fig. 12). Higher porosity should provide more space for NH_3 to diffuse and bind $CaCl_2$, increasing overall sorption capacity and improving mass transfer. In fact, absorption capacities (Fig. 7) suggests that TES activity follows the surface area rank of the samples (Fig. 10). Looking at the RM-$CaCl_2$ combinations (RV, R1, R1KS), one can see that from the virgin case the surface area is substantially higher than in the case of iron (Fig. 12). The exception is the R1K, the $CaCl_2$-RM combination, which has a high activity and a low surface area. High surface area samples after NH_3 treatment could be active enough to easier absorb water and as a result agglomerate, resulting in a decreasing surface area.

Apart from porosity and surface area the thermal conductivity (i.e. heat transfer) of the inductive material can also effect the process. In fact, hematite crystals, identified in XRD analysis of RM, have higher thermal conductivity in comparison with $CaCl_2$ [28,29].

Overall, skull like structures are somewhat present in the iron containing samples, unlike in RM. There is no considerable degradation of the porous structure. Higher magnifications reveal the formation of needle-like large-scale acicular structure, particularly after 1000 cycles (Fig. 12, middle, bottom). Instead, for the red mud-containing samples, fine particles are found to be deposited on the smooth and tight amorphous surface with not-so-well-defined pores (Fig. 11). The tightly sealed iron sample appears to be quite similar to the virgin $CaCl_2$ sample (Figs. 5 and 12). Skull-like structure is still frequent, particularly at higher magnifications, just as in the virgin samples. This is more apparent in the case of iron than in RM. On the contrary, both in iron and RM containing samples, continuous unsealed cycling results in the formation of a highly porous structure of ammonia-$CaCl_2$ adducts.

4. Conclusions

Thermochemical energy storage is a promising technology that can help mitigate demand–supply intermittency issues. Here we investigate

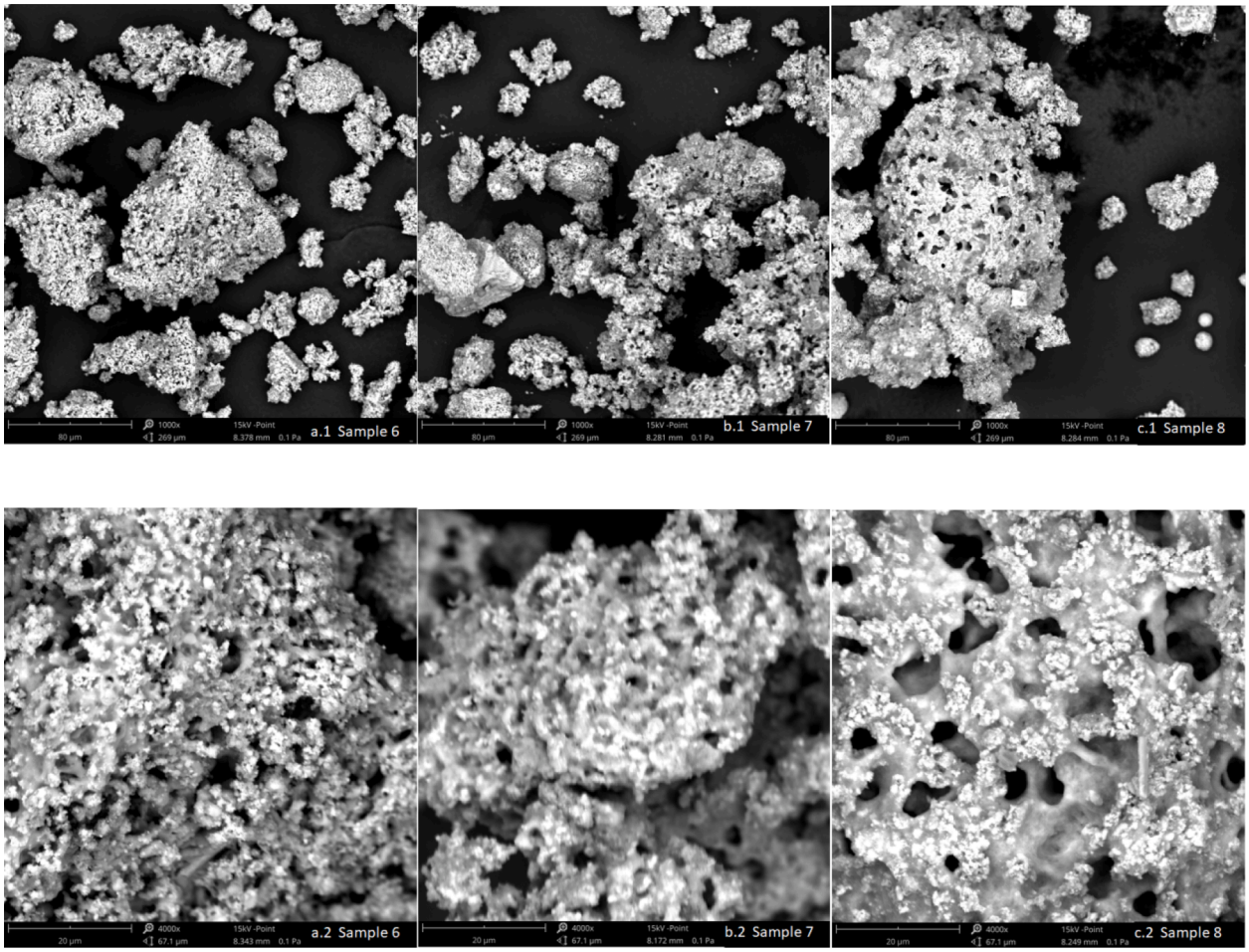

Fig. 11. SEM scans of RM-$CaCl_2$ combinations after cycling. Left to right: R1, R1K, R1KS. Top row magnification is 1000x and bottom 4000x.

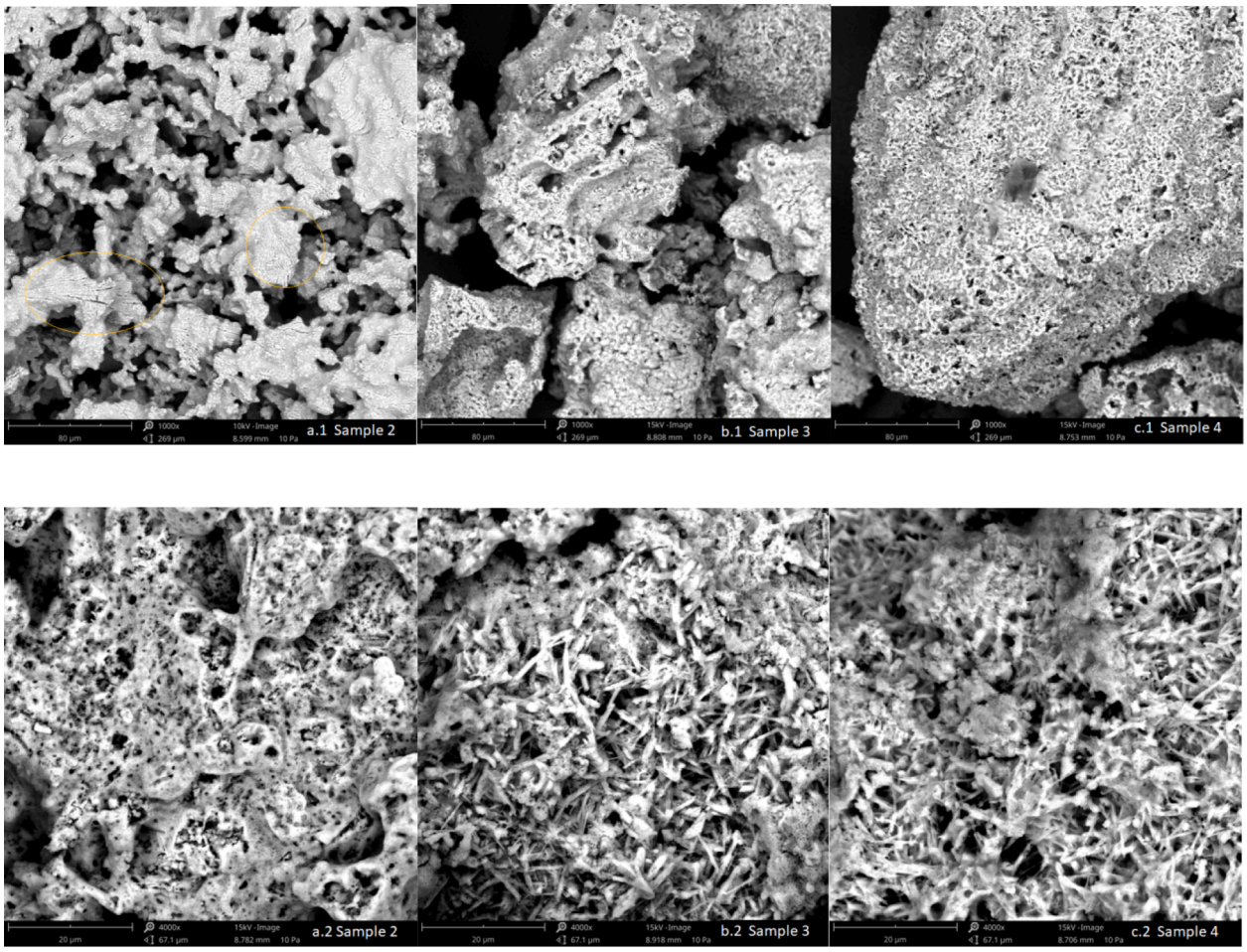

Fig. 12. SEM scans of iron samples after cycling. Left to right: F1, F1K, F1KS. Top row magnification is 1000x and bottom 4000x.

experimentally, for the first time, inductive heating (IH) as a tool for direct power to heat conversion. Among other advantages, IH allows for versatile measurements in rapid multiple adsorption–desorption cycles that have never been used in the TES conversion measurements. Such measurements mimic the natural conditions in actual installations much better than the measurements under the systems heated slowly with the external heat source.

$CaCl_2$-NH_3 is chosen as a material due to the low cost and huge surplus of $CaCl_2$. RM, a disregarded waste of the aluminum industry, and iron wires are used as inductive materials. The following major conclusions are derived from our investigation:

- RM shows satisfactory performance as an inductive material when compared to iron.
- Material showed no signs of degradation after 1000 adsorption/desorption cycles under isochoric conditions. Long-term stability of the system requires further research, but the lack of changes during the testing period allows to believe that the system will also maintain stability over a longer period of operation.
- Samples containing RM showed improved sorption capacity with respect to iron; 0.304 versus 0.154 g_{NH3}/g_{CaCl2}) and desorption enthalpy (716 versus 460 KJ/ kg_{CaCl2}).
- This is found to be related to the higher specific area, on average, of samples containing RM.

Overall, we showed that inductively heated TES with NH_3 could be operated in *in-powder*-$CaCl_2$ with no need of palletizing. Moreover, the system supported by the thermoelectric element could form a close battery-like strategy capable of generating electric power. We hope this work can serve as an onset for more research in inductive thermochemical systems as well as further investigation in the use of RM as an inductive material. Future more thorough investigation towards this direction is quite promising.

CRediT authorship contribution statement

Tomasz Siudyga: . **Karolina Wojtacha-Rychter:** Conceptualization, Methodology, Investigation, Resources, Writing – original draft, Writing – review & editing, Visualization. **Argyrios Anagnostopoulos:** Conceptualization, Methodology, Investigation, Resources, Writing – original draft, Writing – review & editing, Visualization. **Helena Navarro:** Conceptualization, Investigation. **Yulong Ding:** Conceptualization, Investigation. **Adam Smolinski:** Conceptualization, Methodology, Investigation. **Malgorzata Magdziarczyk:** Conceptualization, Investigation. **Pawel Mierczynski:** Conceptualization, Investigation. **Jaroslaw Polanski:** Conceptualization, Methodology, Investigation.

Declaration of Competing Interest

The authors declare that they have no known competing financial interests or personal relationships that could have appeared to influence the work reported in this paper.

Data availability

Data will be made available on request.

Acknowledgments

The work has been performed with the financial support of the National Science Centre (Poland) under OPUS Decisions No. 2018/31/B/ST8/00599 and No. 2018/29/B/ST8/02303. This work was partially supported by the Ministry of Science and Higher Education, Poland [Grant No. 11166012]. The research activities co-financed by the funds granted under the Research Excellence Initiative of the University of Silesia in Katowice, Poland.

References

[1] IEA. Renewables 2020 - Analysis and forecast to 2025. Int Energy Agency 2020.
[2] M. Yekini Suberu, M. Wazir Mustafa, N. Bashir, Energy storage systems for renewable energy power sector integration and mitigation of intermittency, Renew. Sustain. Energy Rev. 35 (2014) 499–514, https://doi.org/10.1016/j.rser.2014.04.009.
[3] H. Zhang, J. Baeyens, G. Cáceres, J. Degrève, Y. Lv, Thermal energy storage: Recent developments and practical aspects, Prog. Energy Combust. Sci. 53 (2016) 1–40, https://doi.org/10.1016/j.pecs.2015.10.003.
[4] J. Cot-Gores, A. Castell, L.F. Cabeza, Thermochemical energy storage and conversion: A-state-of-the-art review of the experimental research under practical conditions, Renew. Sustain. Energy Rev. 16 (2012) 5207–5224, https://doi.org/10.1016/j.rser.2012.04.007.
[5] A.H. Abedin, M.A. Rosen, A Critical Review of Thermochemical Energy Storage Systems, Open Renew Energy J 4 (2011) 42–46, https://doi.org/10.2174/1876387101004010042.
[6] K.E. N'Tsoukpoe, F. Kuznik, A reality check on long-term thermochemical heat storage for household applications, Renew. Sustain. Energy Rev. 139 (2021), 110683, https://doi.org/10.1016/j.rser.2020.110683.
[7] L.F. Marie, S. Landini, D. Bae, V. Francia, T.S. O'Donovan, Advances in thermochemical energy storage and fluidised beds for domestic heat, J Energy Storage 53 (2022), 105242, https://doi.org/10.1016/j.est.2022.105242.
[8] F. Desai, J. Sunku Prasad, P. Muthukumar, M.M. Rahman, Thermochemical energy storage system for cooling and process heating applications: A review, Energy Convers Manag 229 (2021), 113617, https://doi.org/10.1016/j.enconman.2020.113617.
[9] Gunasekara SN, Laios M, Karabanova A, Martin V, Blanchard D. Eurotherm Seminar #112 Advances in Thermal Energy Storage Design of a bench-scale ammonia-SrCl2 thermochemical storage system using numerical modelling n.d. 15-17/05/2019.
[10] M. van der Pal, R.E. Critoph, Performance of $CaCl_2$-reactor for application in ammonia-salt based thermal transformers, Appl. Therm. Eng. 126 (2017) 518–524, https://doi.org/10.1016/j.applthermaleng.2017.07.086.
[11] R.G. Oliveira, R.Z. Wang, C. Wang, Evaluation of the cooling performance of a consolidated expanded graphite–calcium chloride reactive bed for chemisorption icemaker, Int. J. Refrig 30 (2007) 103–112, https://doi.org/10.1016/j.ijrefrig.2006.08.003.
[12] L.W. Wang, R.Z. Wang, J.Y. Wu, K. Wang, Compound adsorbent for adsorption ice maker on fishing boats, Int. J. Refrig 27 (2004) 401–408, https://doi.org/10.1016/j.ijrefrig.2003.11.010.
[13] Y. Sakamoto, H. Yamamoto, Performance of Thermal Energy Storage Unit Using Solid Ammoniated Salt ($CaCl_2$-NH_3 System), Nat Resour 5 (2014) 337–342, https://doi.org/10.4236/nr.2014.58031.
[14] C. Smith, M. Malmali, C.Y. Liu, A.V. McCormick, E.L. Cussler, Rates of Ammonia Absorption and Release in Calcium Chloride, ACS Sustain. Chem. Eng. 6 (2018) 11827–11835, https://doi.org/10.1021/acssuschemeng.8b02108.
[15] G. Zisopoulos, A. Nesiadis, K. Atsonios, N. Nikolopoulos, D. Stitou, A. Coca-Ortegón, Conceptual design and dynamic simulation of an integrated solar driven thermal system with thermochemical energy storage for heating and cooling, J Energy Storage 41 (2021), 102870, https://doi.org/10.1016/j.est.2021.102870.
[16] A. Bloess, W.P. Schill, A. Zerrahn, Power-to-heat for renewable energy integration: A review of technologies, modeling approaches, and flexibility potentials, Appl. Energy 212 (2018) 1611–1626, https://doi.org/10.1016/j.apenergy.2017.12.073.
[17] S. Ceylan, C. Friese, C. Lammel, K. Mazac, A. Kirschning, Inductive heating for organic synthesis by using functionalized magnetic nanoparticles inside microreactors, Angew Chemie - Int Ed 47 (2008) 8950–8953, https://doi.org/10.1002/anie.200801474.
[18] T. Siudyga, M. Kapkowski, P. Bartczak, M. Zubko, J. Szade, K. Balin, et al., Ultra-low temperature carbon (di)oxide hydrogenation catalyzed by hybrid ruthenium–nickel nanocatalysts: towards sustainable methane production, Green Chem. 22 (2020) 5143–5150, https://doi.org/10.1039/d0gc01332c.
[19] S. Vigneshwaran, M. Uthayakumar, V. Arumugaprabu, Potential use of industrial waste-red mud in developing hybrid composites: A waste management approach, J. Clean. Prod. 276 (2020), 124278, https://doi.org/10.1016/j.jclepro.2020.124278.
[20] T.A. Zhang, Y. Wang, G. Lu, Y. Liu, W. Zhang, G. Zhao, Comprehensive utilization of red mud: Current research status and a possible way forward for non-hazardous treatment, Miner Met Mater Ser (2018) 135–141, https://doi.org/10.1007/978-3-319-72284-9_18.
[21] B. Swain, A. Akcil, J. Lee, Red mud valorization an industrial waste circular economy challenge; review over processes and their chemistry, Crit. Rev. Environ. Sci. Technol. 52 (2022) 520–570, https://doi.org/10.1080/10643389.2020.1829898.
[22] S. Wang, H. Jin, Y. Deng, Y. Xiao, Comprehensive utilization status of red mud in China: A critical review, J. Clean. Prod. 289 (2020), 125136, https://doi.org/10.1016/j.jclepro.2020.125136.
[23] A. Suryawanshi, V. Aravindan, S. Madhavi, S. Ogale, Red Mud and Li-Ion Batteries: A Magnetic Connection, Chem Sus Chem. 9 (2016) 2193–2200, https://doi.org/10.1002/cssc.201600561.
[24] A. Anagnostopoulos, M.E. Navarro, M. Stefanidou, Y. Ding, G. Gaidajis, Red mud-molten salt composites for medium-high temperature thermal energy storage and waste heat recovery applications, J. Hazard. Mater. 413 (2021), 125407, https://doi.org/10.1016/j.jhazmat.2021.125407.
[25] A. Anagnostopoulos, M.E. Navarro, M. Stefanidou, P. Seferlis, G. Gaidajis, Y. Ding, Effect of carbon on the performance of red mud-molten salt composites for thermal management and waste heat recovery applications, J Energy Storage 44 (2021), 103363, https://doi.org/10.1016/j.est.2021.103363.
[26] G. Diguet, E. Beaugnon, J.Y. Cavaillé, Shape effect in the magnetostriction of ferromagnetic composite, J Magn Mater 322 (2010) 3337–3341, https://doi.org/10.1016/j.jmmm.2010.06.020.
[27] X. Liu, P. Gao, S. Yuan, Y. Lv, Y. Han, Clean utilization of high-iron red mud by suspension magnetization roasting, Miner. Eng. 157 (2020), 106553, https://doi.org/10.1016/j.mineng.2020.106553.
[28] J.M.H. Hendrickx, J.B.J. Harrison, R.L. van Dam, B. Borchers, D.I. Norman, C.D. Dedzoe, et al. Magnetic soil properties in Ghana, Proc. SPIE 5794, Detection and Remediation Technologies for Mines and Minelike Targets X, (10 June 2005). Doi: 10.1117/12.603416.
[29] E. Vainio, N. Demartini, L. Hupa, L.E. Åmand, T. Richards, M. Hupa, Hygroscopic Properties of Calcium Chloride and Its Role on Cold-End Corrosion in Biomass Combustion, Energy Fuel 33 (2019) 11913–11922, https://doi.org/10.1021/acs.energyfuels.9b02731.
[30] M. Gaeini, A.L. Rouws, J.W.O. Salari, H.A. Zondag, C.C.M. Rindt, Characterization of microencapsulated and impregnated porous host materials based on calcium chloride for thermochemical energy storage, Appl. Energy 212 (2018) 1165–1177, https://doi.org/10.1016/j.apenergy.2017.12.131.
[31] K. Wagner, M. Malmali, C. Smith, A. McCormick, E.L. Cussler, M. Zhu, et al., Column absorption for reproducible cyclic separation in small scale ammonia synthesis, AIChE J 63 (2017) 3058–3068, https://doi.org/10.1002/aic.15685.
[32] M. Malmali, G. Le, J. Hendrickson, J. Prince, A. McCormick, E.L. Cussler, Better Absorbents for Ammonia Separation, ACS Sustain. Chem. Eng. 6 (2018) 6536–6546, https://doi.org/10.1021/acssuschemeng.7b04684.
[33] L.F. Cabeza, A. Solé, C. Barreneche, Review on sorption materials and technologies for heat pumps and thermal energy storage, Renew. Energy 110 (2017) 3–39, https://doi.org/10.1016/j.renene.2016.09.059.
[34] Landolt-Börnstein., Thermodynamic Properties of Inorganic Material, Springer-Verlag, Berlin-Heidelberg, 1999.
[35] A. Bard, R. Parsons, J. Jordan, Standard Potentials in Aqueous Solution. (1985), https://doi.org/10.1201/9780203738764.
[36] R. Wang, L. Wang, J.Y. Wu, Mechanism and Thermodynamic Properties of Chemical Adsorption. (2014), https://doi.org/10.1002/9781118197448.ch4.
[37] Y. Yang, M. Faheem, L. Wang, Q. Meng, H. Sha, N. Yang, et al., Surface Pore Engineering of Covalent Organic Frameworks for Ammonia Capture through Synergistic Multivariate and Open Metal Site Approaches, ACS Cent. Sci. 4 (2018) 748–754, https://doi.org/10.1021/acscentsci.8b00232.
[38] X. Tian, J. Qiu, Z. Wang, Y. Chen, Z. Li, H. Wang, et al., A record ammonia adsorption by calcium chloride confined in covalent organic frameworks, Chem. Commun. 58 (2022) 1151–1154, https://doi.org/10.1039/d1cc06308a.